Volume 4, Issue 2, pp 44-57, March, 2023

ACHIEVERS JOURNAL OF SCIENTIFIC RESEARCH
Open Access Publications of Achievers University, Owo
Available Online at *www.achieversjournalofscience.org*

Statistical Model for Melting Heat Transfer in Micropolar Nanofluid Flow over an Electromagnetic Actuator with Irregular Thickness

Fatunmbi, E.O.[1*] and Aako, O. L.[2]

[1-2]Department of Mathematics and Statistics, Federal Polytechnic, Ilaro, Nigeria.
Corresponding author e-mail: ephesus.fatunmbi@federalpolyilaro.edu.ng

Submitted: December 15, 2022; Revised: January 22, 2023; Accepted: February, 20, 2023; Published: March, 20, 2023

Abstract

This article analyses statistical model mechanism in the motion of micropolar nanofluid over an electromagnetic actuator with variable thickness. The formulated model captures melting heat transfer phenomenon coupled with thermal radiation, viscous dissipation, thermal-movement and Brownian motion of nanoparticles. The model equations are restructured into ordinary derivatives from the initial partial derivatives by means of relevant similarity quantities. The equations are subsequently tackled numerically via shooting technique alongside Runge-Kutta Fehlberg scheme. The results are displayed graphically to showcase the contributions of the physical terms emerging from the model on the dimensionless quantities. In the analysis, it is found that an enhancement in the magnitude of the melting heat parameter reduces the surface heat propagation but viscous dissipation term acts contrary. Besides, augmenting the magnitude of micropolar and modified Hartmann number parameters boosts the fluid motion. More so, various statistical models are applied to test the data set for the coefficient of skin friction and the Nusselt number for variations in the micropolar fluid parameter (K). The statistical analysis points out that the data set for skin friction coefficient fits the Frechet model for $K = 0$ and the Weibull model for $K = 1,2,3$ whereas that of the Nusselt number fits the Frechet distribution for $K = 0, 1$ and Lognormal distribution for $K = 2$ & 3.

Keywords: Electromagnetic actuator, Microplar nanofluid; Melting heat transfer; Statistical model, Thermophoresis

1.0 Introduction

Eringen (1966, 1972) conceputualized the concept of micropolar fluid and thermo-micropolar fluid respecticvely. Micropolar fluid is a branch of non-Newtonian fluid which posses microstructures with a unique characteristics of randomly oriented or rigid spherical particles. This fluid model accurately captures the flow mechanism of animal blood, liquid crystals, polymeric suspensions, colloidal fluids and exotic lubricants (Lukaszewicz, 1999; Hayat *et al*., 2008; Chen *et al*., 2011, Fatunmbi and Adeniyan, 2018). Due to wide-ranging engineering and industrial applications derivable from micropolar fluid, various researchers have paid attention to investigate its flow mechanism

as well as its dynamics of heat transfer under diverse conditions and configurations. Its applications can be encountered in paint rheology and chemical engineering, bio-mechanics engineering (e.g. motion of blood in the body, fluid movement in the brain, etc.), the cooling of metallic sheet in water bath, etc. (Rahman, 2009; Reena and Rana, 2009).

In different areas of manufacturing and engineering processes (e. g. transportation processes, pharmaceutical and drug delivery, cancer treatment, etc.), the concept of heating and cooling are often encountered. Hence, it becomes essential to investigate the thermal properties of various devices for better performance. The suspension of nanometer-sized particles in the convectional fluid (such as: water, kerosene, oil, ethlene glycol, etc.) to form a colloidal solution of nanoparticles in the base fluid is termed nanofluid. Usually, these nanoparticles are typically made of metals, oxides, carbides, or carbon nanotubes, This new class of fluids have the capacity to enhance the thermal conduction as well as the thermo-physical fluid properties (viscosity, thermal conductivity, thermal diffusivity, heat transfer). Choi (1995) initiated such a concept and due to wide applications of such phenomenon, various researchers have reported on their flow mechanism. Noor *et al*. (2015) carried out an analysis on the mixed convection of a micropolar nanofluid towards a stagnation point over an elongated surface. Their investigation showed that the blend of convectional fluid and the nanoparticles produced an enhanced heat transfer mechanism. Gangadhar *et al*. (2017) employed a numerical approach to evaluate the motion of magneto-micropolar nanofluid on a two dimensional stretching/shrinking material with surface mass flux featuring Newtonian heating condition. Subhani and Nadeem (2018) inspected the thermal characteristics and motion of micropolar hybrid nanoliquid in a porous material surface. The study showed that heat transfer in a hybrid naoliquid is higher than that of nanofluid in the presence of microrotation effects. Atif *et al*. (2019) examined bioconvective motion of micropolar fluid with the mixture of nanoparticles consisting motile microorganism and wall stratification. The authors pointed out that a rise in the micropolar material parameter caused a decline in the thermal field as well concentration profile. Recently, Fatunmbi and Salawu (2021) discussed a numerical analysis of chemically reacting micropolar nanofluid motion featuring viscous dissipation and multiple slips effects at the wall. The authors reported a shrinking concentration boundary layer but an enlarged momentum boundary structure in the presence of Brownian motion parameter. Of recent, Fatunmbi *et al*. (2021) evaluated heat transfer characteristics in the motion of tangent hyperbolic nanofluid over a permeable expanding plate in the neighbourhood of a stagnation point in the presence of nonlinear mixed convection term. The researchers reported a drop in the heat transfer rate due to impovement in the magnitude of thermophoresis and the Brownian motion terms.

In engineering science such as in geophysics and astrophysics, the use of magnetic fields for the control of electro-conducting fluids as liquid metals, plasmas, etc. is important. However, when the electrical conductivity of the fluid is low, there is a need to introduce external electric field because the external magnetic field currents alone cannot induce efficient flow mechanism in such scenarios. A device known as electromagnetic actuator (Riga plate) can be used to induce the required flow current. In this device, there is arrangement of fixed alternating electrodes and magnets placed on the surface such that the Lorentz force is generated parallel to the plane. This idea was originated by Gailitis and Lielausis (1961) and has been extended by many scholars (Abbas *et al*., 2016; Fatunmbi and Adeosun, 2020; Fatunmbi *et al*., 2021). In all of these studies however, the application of statistical models to test the data set for the engineering quantities of interest (skin friction coefficient and the Nusselt number) and to fit the best distribution for variations in the fluid material property has not been considered. This becomes necessary to accurately predict the pattern of flow and heat transfer behaviour of

fluid material property for applications in various industrial activities.

Hence, the intent of the current study is to establish statistical model for the flow and melting heat transfer in micropolar nanoliquid over an electromagnetic actuator with variable thickness. The developed model features the effects of viscous dissipation, thermal radiation and temperature-reliant thermal conductivity. This study therefore intends to provide answers to the following research questions. How does the modified Hartmann number affect the flow and thermal fields of the micropolar nanoliquid?

Is there a significant impact of the variable thickness and melting heat transfer on the flow and thermal field of micropolar nanoliquid? Which statistical distribution model provides the best fit for the skin friction coefficient for variation in the micropolar fluid material? Which statistical distribution model provides the best fit for Nusselt number (heat transfer) for variation in the micropolar fluid material?

To provide answers to aforementioned questions, the controlling equations have been numerically integrated via the approach of shooting technique and associated with Runge-Kutta Fehlberg algorithm. Afterwards, various graphs have been plotted and tables generated to discuss the effects of the pertinent parameters affecting the flow dynamics and heat transfer mechanism.

2 Problem Development

An incompressible, steady motion and melting heat transfer of micropolar nanofluid over an electromagnetic actuator with variable thickness is considered. In the development of this problem, there is an assumption viscous dissipation, thermophorseis and Brownian motion effects are present whereas the thermal conductivity relies on the temperature. The direction of motion is in x axis while y direction is fixed perpendicular to it with respective components of velocity indicated as u and v as displayed in figures 1a & 1b. The sheet is stretching with the velocity $u = u_w(x) = a(x+w)^n$.

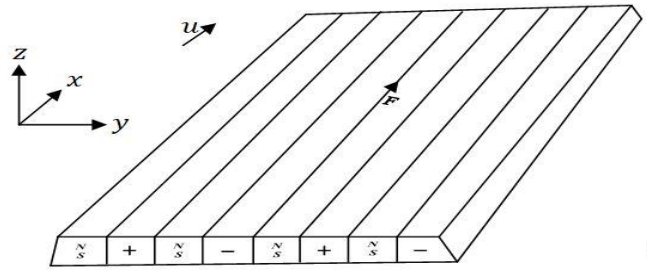

Figure 1a: Electromagnetic actuator

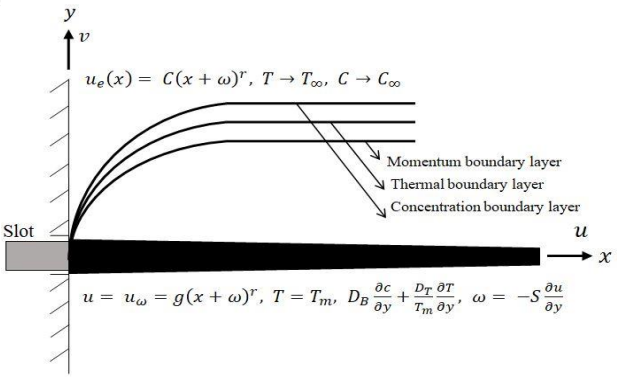

Figure 1b: Flow configuration and coordinate system

The sheet is not flat as described in Fig. 1b. with a given profile which is specified as $y = b(x+w)^{(1-n)/2}$, where b is taken so small for the sheet to be suitably thin. This problem is valid for $r \neq 1$ since r = 1 depicts a flat sheet case. In the boundary conditions, the stretching surface temperature and concentration are higher than that of the free stream. i.e . $T_w > T_\infty$ and $C_w > C_\infty$.

2.1 The Governing Equations

In line with the above-mentioned assumptions, the equations governing the problem are communicated as follows (see Fatunmbi and Adeosun, 2020; Iqbal *et al*., 2017):

$$\frac{\partial u}{\partial x} + \frac{\partial v}{\partial y} = 0, \tag{1}$$

$$u\frac{\partial u}{\partial x} + v\frac{\partial u}{\partial y} = (\mu + \kappa)\frac{\partial^2 u}{\partial y^2} + \frac{\kappa}{\rho}\frac{\partial N}{\partial y} + \frac{\pi j_0 M_o}{8\rho}\exp\left(-\frac{\pi}{h}y\right), \tag{2}$$

$$u\frac{\partial N}{\partial x}+v\frac{\partial N}{\partial y}=\frac{\gamma}{\rho j}\frac{\partial^2 N}{\partial y^2}-\frac{\kappa}{\rho j}\left(2\mathrm{N}+\frac{\partial u}{\partial y}\right), \tag{3}$$

$$u\frac{\partial T}{\partial x}+v\frac{\partial T}{\partial y}=\frac{1}{\rho c_p}\frac{\partial}{\partial y}\left(k\frac{\partial T}{\partial y}\right)+\Upsilon\left[\frac{D_T}{T_\infty}\left(\frac{\partial T}{\partial y}\right)^2+D_b\left(\frac{\partial T}{\partial y}\frac{\partial C}{\partial y}\right)\right]+\frac{(\mu+\kappa)}{\rho c_p}\left(\frac{\partial u}{\partial y}\right)^2+\frac{16\sigma^\star T_\infty^3}{3k_\star\rho c_p}\frac{\partial^2 T}{\partial y^2}, \tag{4}$$

$$u\frac{\partial C}{\partial x}+v\frac{\partial C}{\partial y}=D_b\frac{\partial^2 C}{\partial y^2}$$

$$+\frac{D_T}{T_\infty}\left(\frac{\partial^2 T}{\partial y^2}\right). \tag{5}$$

Subject to the following boundary conditions:

$$\begin{aligned}&u=u_w(x)=a(x+w)^n, v=0, T=T_m, D_b\frac{\partial C}{\partial y}+\frac{D_T}{T_m}\frac{\partial T}{\partial y}=0, N=-m\frac{\partial u}{\partial y},\\&k\left(\frac{\partial T}{\partial y}\right)=\rho[\lambda_1+C_s(T_m-T_0)]v(x,0)\ \ at\ \ y=b(x+w)^{(1-n)/2},\\&u\to 0, T\to T_\infty, C\to C_\infty\ \ y\to\infty.\end{aligned} \tag{6}$$

The variation of the thermal conductivity with temperature is expressed as (see Hayat et .al, 2018)

$$k=k_\infty\left(1+L\frac{T-T_m}{T_\infty-Tm}\right). \tag{7}$$

The quantities in Eq. (8) are introduced into the main equations to transform them from partial to ordinary differential equations (see Hayat et .al, 2018).

$$K=\left(\frac{\kappa}{\mu}\right), Ec=\left(\frac{u_w^2}{c_p(T_\infty-T_m)}\right),\quad Le=\left(\frac{\alpha}{D_b}\right), \epsilon=\left[\frac{\pi}{h}\left(\frac{2\nu(x+w)^{1-n}}{(r+1)a}\right)^{\frac{1}{2}}\right],\quad Nt=\frac{D_T\Upsilon(T_\infty-T_m)}{\nu T_\infty},\quad \alpha=\left(\frac{k}{(\mu c_p)}\right),\quad \xi=y\left[\frac{(n+1)}{2\nu}a(x+w)^{n-1}\right]^{\frac{1}{2}}, u=\mathrm{a}(x+w)^n F'(\xi), N=G(\xi)\left[\frac{a^3(n+1)(x+w)^{(3n-1)}}{2\nu}\right]^{\frac{1}{2}}, Pr=\left(\frac{\nu}{\alpha}\right),\quad Nb=\frac{D_b\Upsilon C_\infty}{\nu}, v=-\left[\frac{a\nu(r+1)}{2}(x+w)^{(r-1)}\right]^{\frac{1}{2}}\left(F(\xi)+\frac{(n-1)}{(r+1)}\eta F'(\xi)\right), \mathrm{Z}=\left(\frac{c_p(T_\infty-T_m)}{[\lambda_1+C_s(T_m-T_0)]}\right), \gamma=\left(\mu+\frac{\kappa}{2}\right)j,\quad j=\left(\frac{\nu}{n}\right)x^{(1-n)}., \Phi(\eta)=\frac{C}{C_\infty},$$

$$\mathrm{v}=-\left[\frac{a\nu(n+1)}{2}(x+w)^{(r-1)}\right]^{\frac{1}{2}}\left(F(\xi)+\frac{(n-1)}{(n+1)}\eta F'(\xi)\right),$$

$$\epsilon=\left[\frac{\pi}{h}\left(\frac{2\nu(x+w)^{1-r}}{(r+1)a}\right)^{1/2}\right], \mathrm{M}=\left(\frac{\pi j_0 M_0}{8\rho q^2(x+w)^{2r-1}}\right), Nr=\frac{16\sigma^\star T_\infty}{\mathrm{k}_\infty k^*}, \epsilon=(1+\mathrm{L}\theta). \tag{8}$$

The governing equations therefore translate to the underlisted equations in view of Eqs. (7) and (8).

$$(1+K)F'''-\left(\frac{2r}{r+1}\right)F'^2+FF'+Kg'+\left(\frac{2}{r+1}\right)Me^{-\eta\epsilon}=0, \tag{9}$$

$$(1+K/2)G''+FG'-\left(\frac{3r-1}{r+1}\right)F'g-K(2g+F'')\left(\frac{2}{r+1}\right)=0, \tag{10}$$

$$(1+Nr+\epsilon\Theta)\Theta''+\epsilon\Theta'^2+\mathrm{Pr}\,(F\Theta'+Ec(1+K)F''^2+Nt\Theta'^2+Nb\Theta'\Phi')=0, \tag{11}$$

$$\Phi''+\frac{NT}{Nb}\Theta''+PrLeF\Phi'=0. \tag{12}$$

Subject to:

$$\begin{aligned}&F'(\beta)=1, \Theta(\beta)=0, \Phi(\beta)=0, G=-mF''(\beta)\ \ at\ \ \beta=b\left(\frac{(r+1)n}{2\nu}\right)^{1/2}\\&Z\Theta'(\beta)+PrF(\beta)=\beta\left(\frac{1-n}{1+n}\right)F'(\beta)\ \ at\ \ \beta=b\left(\frac{(r+1)n}{2\nu}\right)^{1/2}\\&F'(\infty)\to 0, \Theta(\infty)\to 1, \Phi(\infty)\to 1\ \ as\ \ a\to\infty.\end{aligned} \tag{13}$$

In Eqs. (9-13), the differentiation is done with respect to ξ, $\beta = \left(b\left(\frac{(n+1)a}{2\nu}\right)^{1/2}\right)$ is the wall thickness term and $\xi = \beta = a\left(\frac{(n+1)\kappa}{2\nu}\right)^{1/2}$ denotes flat surface. In order to convert the domain into $[0,\infty]$, it is assumed that $F(\xi) = f(\xi - \beta) = f(\eta)$, $G(\xi) = g(\xi - \beta) = g(\eta)$, $\Theta(\xi) = \theta(\xi - \beta) = \theta(\eta)$ and $\Phi(\xi) = \phi(\xi - \beta) = \phi(\eta)$, with these relations, the outlinig equations simplify to:

$$(1+K)f''' - \left(\frac{2n}{n+1}\right)\mathrm{f}'^2 + ff'' + Kg' + \left(\frac{2}{n+1}\right)Me^{-(a+\eta)h} = 0, \tag{14}$$

$$(1+K/2)g'' + fg' - \left(\frac{3n-1}{n+1}\right)f'g - K(2g+f'')\left(\frac{2}{n+1}\right) = 0, \tag{15}$$

$$(1+Nr+L\theta)\theta'' + L\theta'^2 + Prf\theta' + PrEc(1+K)f''^2 + PrNt\theta'^2 + PrNb\theta'\phi' = 0 \tag{16}$$

$$\phi'' + \frac{Nt}{Nb}\theta'' + PrLef\phi' = 0. \tag{17}$$

Subject to:
$$\begin{aligned} &at\ \eta = 0 \quad f' = 1, \theta = 0, g = -mf'', \phi = 0, f = 1/\mathrm{Pr}\left[a\left(\frac{1-n}{1+n}\right) - Z\theta'\right] \\ &as\ \eta \to \infty \quad f' \to 0, g \to 0, \theta \to 1, \phi \to 1. \end{aligned} \tag{18}$$

Table 1: Nomenclature

Symbol	Description	Symbol	Description
u, v	velocity in x, y direction	T_m	melting temperature
ρ	fluid density viscosity	h	width of magnets and electrodes
μ	dynamic viscosity	ν	fluid kinematic viscosity
κ	vortex viscosity	λ_1	latent fluid heat
T	Fluid temperature	k^*	mean absorption coefficient
(ρc_p)	heat capacity	C_s	heat capacity of concentration surface
$a^\star$	Stefan-Boltzmann constant	T_0	solid surface temperature
T_∞	temperature at free stream	m	boundary parameter
k	Fluid thermal conductivity	D_b	molecular diffusivity
j	micro inertia density	D_T	Thermophoresis coefficient
L	thermal conductivity parameter	N	component of micro rotation
u_w	stretching velocity	γ	spin gradient viscosity
M	Modified Hartmann number	Z	Melting heat parameter
Ec	Eckert number	Le	Lewis number
K	Micropolar parameter	Nt	Thermophoresis term
Pr	Prandtl number	Nb	Brownian motion parameter
ϵ	Dimensionless parameter	n	Power law index

3. Numerical Method.

A numerical solution of the set of the boundary value problem Eqs. (14-18) has been sought due to strong nonlinearity of the problem. An unconditionally stable numerical solution via Runge-Kutta-Fehlberg scheme alongside with the shooting technique is employed. The detailed procedure of this method can be obtained in Xu and Lee (2013); Mahanthesh *et al*. (2018); Fatunmbi and Okoya (2020).

3.1 Statistical Model selection

In this study, Akaike Information Criterion (AIC) and Bayesian Information Criterion (BIC) are employed to select the best statistical model (Shafiq *et al*., 2021). The data for the skin friction coefficient C_{fx} and the Nusselt number

Nu_x are tested using AIC and BIC. The model that fits best to the data among basic statistical models listed in Table 2 is then determined via AIC and BIC for each model in the table. The distribution with the lowest BIC/AIC value is adjudged the best fitted.

The respective formula for AIC and BIC are:

$AIC = -2\log(s) + 2c$ and $BIC = -2\log(s) + clog(n)$

Where s indicates the model likelihood function and c denotes number of parameters.

3.0 Results and Discussion

The effects of some selected physical parameters on the velocity field and heat distribution are graphically presented and discussed in this section. Figure 2 describes the impact of melting heat transfer M on the velocity. It is noticed that the fluid velocity enhances with growth in the magnitude of the melting parameter M within the boundary layer region.

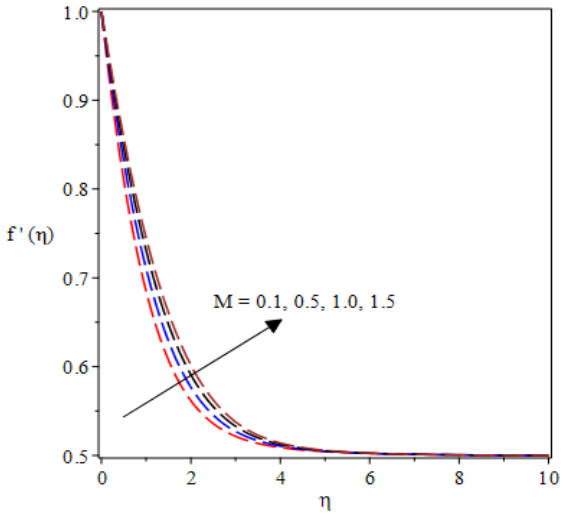

Fig. 2: Effects of M on velocity profile

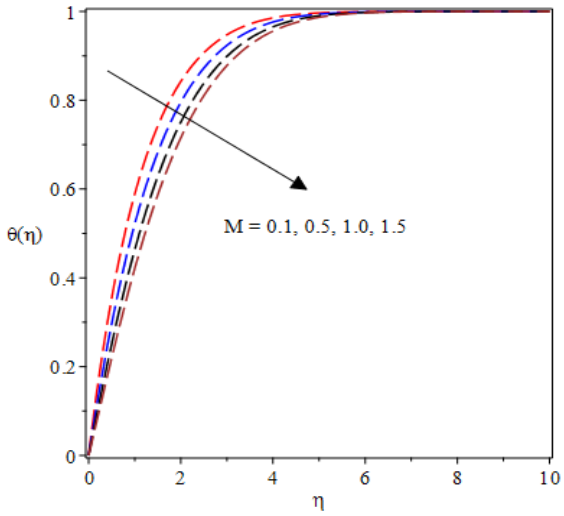

Fig. 3: Plot of M on temperature

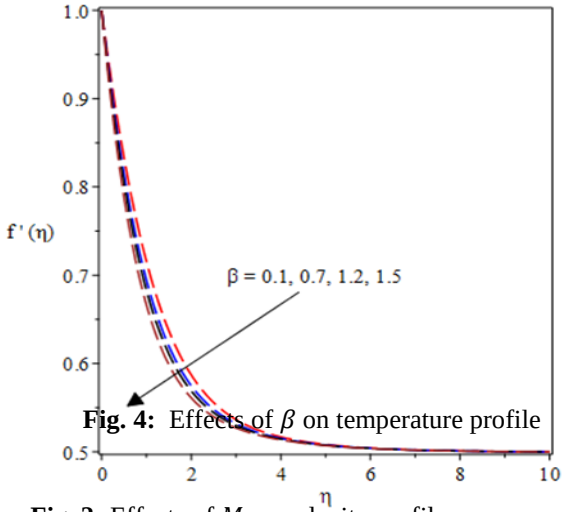

Fig. 4: Effects of β on temperature profile

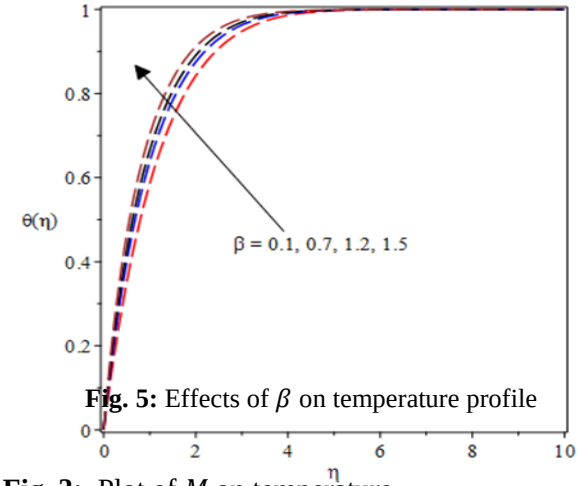

Fig. 5: Effects of β on temperature profile

This trend is attributed to the movement of the solid surface and the free stream in the same direction. Conversely, the thermal field witnesses a decrease in the heat distribution with growing values of M as depicted in Fig. 3

Figure 4 portrays the reaction of the velocity profile for growth in different values of the wall thickness parameter β. A decreased in the fluid motion is observed as the wall thickness parameter β rises. An increase in β depletes the momentum boundary layer structure which in turn propels a slow motion. It is shown that the velocity profile manifests a decreasing pattern with an increment in the wall thickness term

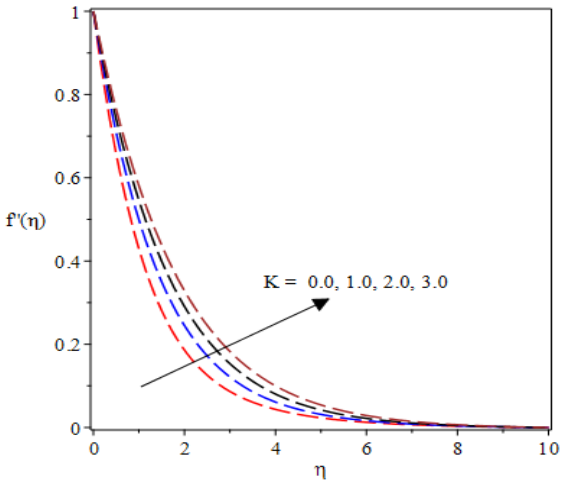

Fig. 6. Effects of K on temperature profile

temperature distribution increases as β. A rise in the magnitude of the micropolar material parameter K promotes an increase in the velocity profile as seen in Fig. 6. This is an indication that there is a reduction in the dynamic fluid viscosity as K increases. Nevertheless, the temperature distribution reduces for higher magnitudes of K as observed in Fig. 7.

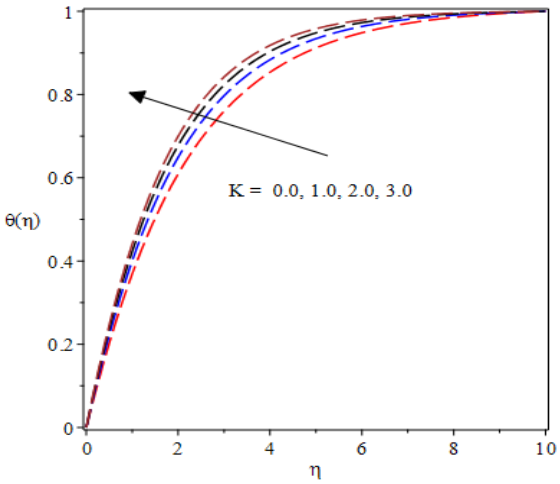

Fig. 7. Effects of K on temperature profile

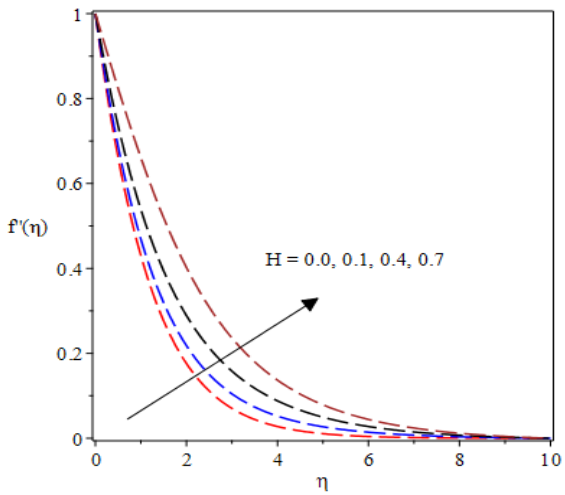

Fig. 8. Effects of H on temperature profile

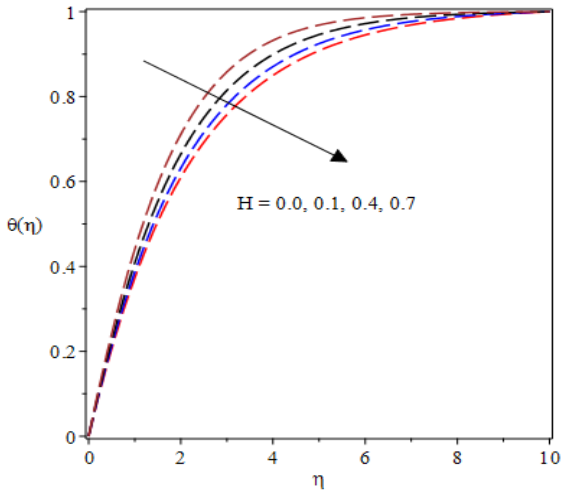

Fig. 9. Effects of H on temperature profile

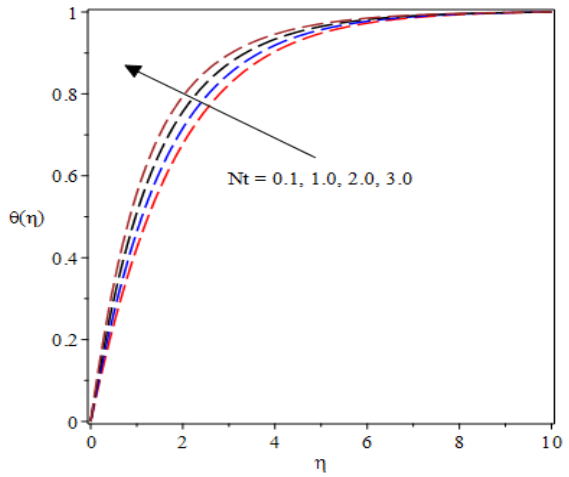

Fig. 10. Effects of Nt on temperature profile

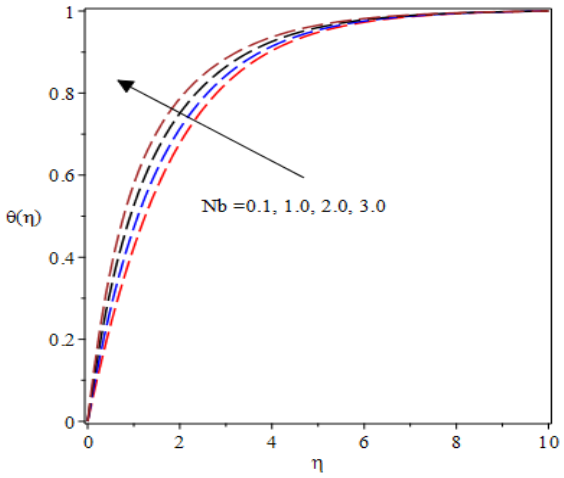

Fig. 11. Effects of Nb on temperature profile

Figure 8 depicts the graph of the velocity profile for variation in the modified Hartmann number H. It is noticed that growing values of H boosts the hydrodynamic boundary layer and accelerates the fluid motion. The Lorentz force parallel to the wall induces current in the fluid such that there is a higerrr velocity due to rising values of H.

Figure 10 elucidates the impact of the thermophoresis parameter on the temperature profile $\theta(\eta)$.. It is evident that growing values of Nt boosts the surface temperature as depicted in this figure. The thermal field expands due to thermophoresis occurrence owing to Brownian motion of the nanoparticles in fluids with a constant gradient of temperature. Similarly, the heat distribution also increases due to a rise in the Brownian motion which characterizes the haphazard motion of the nanoparticles as shown in Fig. 11.

The data for the skin friction coefficient and Nusselt were further analyzed on the basis of Fig. 12 and 13, in order to obtain the statistical properties for the tested models. Tables 3 and 5 present the estimated parameters of the different distributions that have been tested with the considered data. Tables 4 and 6 give the AIC and BIC for the C_{fx} and Nu_x numbers. The result of AIC and BIC show that data set for C_{fx} fits the Frechet model for $K = 0$ and the Weibull model for $K = 1,2,3$. On the other hand, Nu_x data set fits the Frechet distribution well for $K = 0,1$ and the Lognormal distribution for $K = 2,3$. This is an indication that the form of the distribution changes after $K = 0$ for C_{fx} and $K = 1$ for Nu_x respectively. Figures 12 and 13 show the estimated densities using data of C_{fx} and Nu_x under the models in Table 1 which corroborate the results of the AIC and BIC.

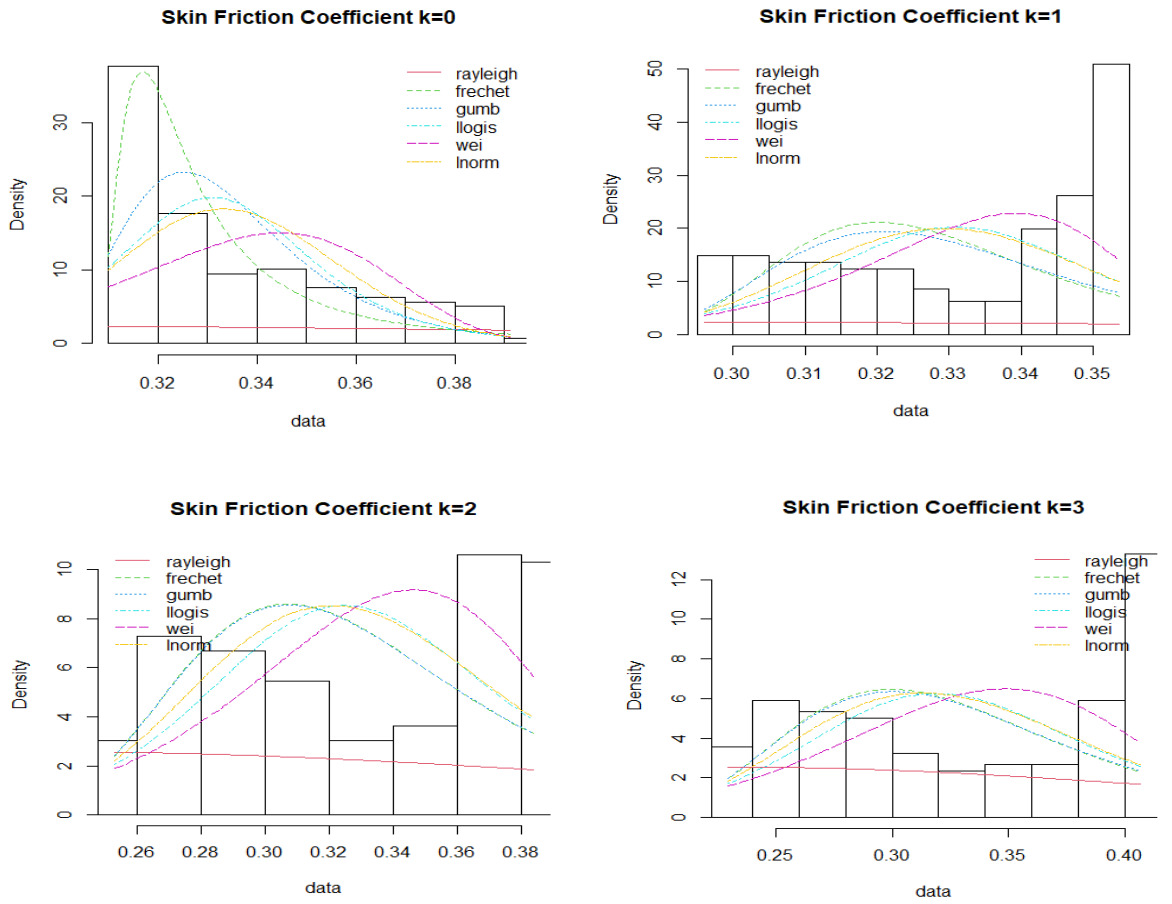

Fig. 12: The estimated densities for the skin friction coefficient C_{fx}

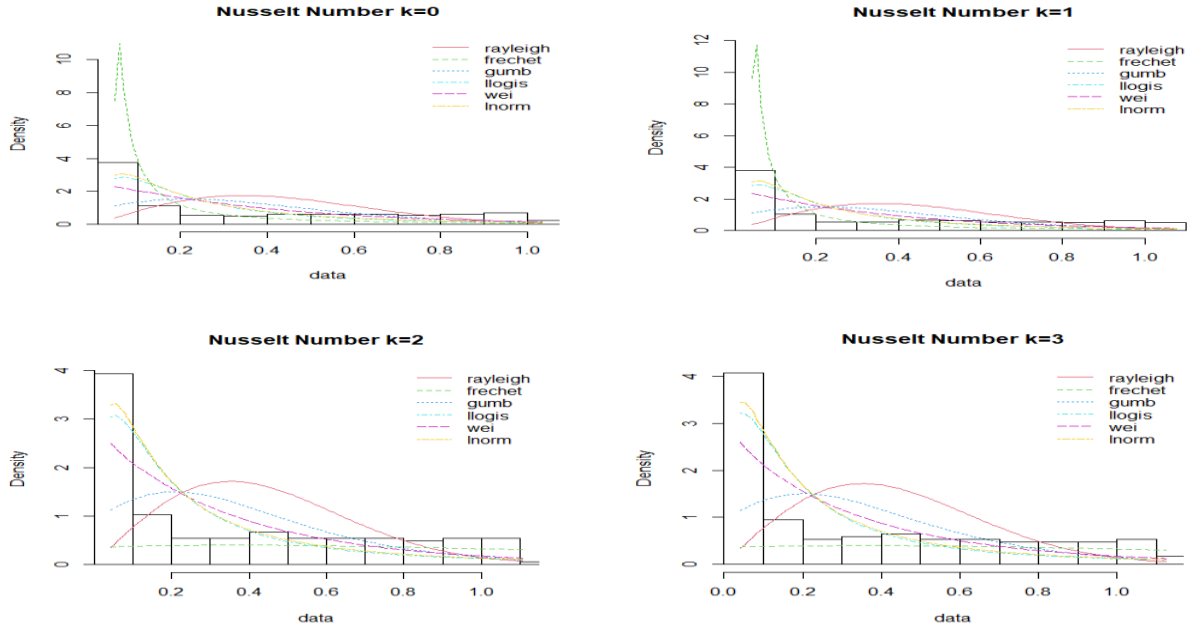

Fig. 13: The estimated densities for the Nusselt number Nu_x

Table 2: The test distribution for skin friction coefficient C_{fx} and Nusselt number Nu_x

Distribution	Probability distribution function $\boldsymbol{f(x)}$
Rayleigh	$f(x,\sigma) = \frac{x}{\sigma^2} e^{-\frac{x^2}{2\sigma^2}} \;;\; x > 0, \sigma > 0$
Fre'chet	$f(x,\alpha,s,m) = \frac{\alpha}{s}\left(\frac{x-m}{s}\right)^{-1-\alpha} e^{-\left(\frac{x-m}{s}\right)^{-\alpha}} \;;\; x > m,\ \alpha > 0, s > 0$
Gumbel	$f(x,\mu,\beta) = e^{-(z+e^{-z})} \;\; where \;\; z = \frac{x-\mu}{\beta} \;;\; \mu > 0, \beta > 0$
Log-logistic	$f(x,\alpha,\beta) = \frac{\left(\frac{\beta}{\alpha}\right)\left(\frac{x}{\alpha}\right)^{\beta-1}}{\left(1+\left(\frac{x}{\alpha}\right)^{\beta}\right)^2} \;;\; x > 0, \alpha > 0, \beta > 0$
Weibull	$f(x,\lambda,k) = \frac{k}{\lambda}\left(\frac{x}{\lambda}\right)^{k-1} e^{-\left(\frac{x}{\lambda}\right)^k} \;;\; x > 0, \lambda > 0, k > 0$
Log-normal	$f(x,\sigma,\mu) = \frac{1}{x\sigma\sqrt{2\pi}} e^{\left(-\frac{(\ln x-\mu)^2}{2\sigma^2}\right)} \;\; \sigma > 0, \mu > 0$

Table 3: Parameter estimates for the statistical distribution of C_{fx}

Skin friction coefficient C_{fx}					
Distribution	Parameter	$K = 0$	$K = 1$	$K = 2$	$K = 3$
Rayleigh	σ	0.2376	0.2345	0.2363	0.2392
Frechet	m	0.3008	-97251.9	-39700.7	-2042024
	s	0.0206	97252.2	39701.0	2042024
	α	1.8112	5586371.1	927900.6	35887025
Gumbel	μ	0.3252	0.3209	0.3073	0.3001
	β	0.0158	0.0190	0.0431	0.0579
Log-logistic	β	26.3002	26.8173	11.1662	8.1042
	α	0.3320	0.3319	0.3300	0.3289
Weibull	k	14.105	21.0749	8.6823	6.2428
	λ	0.3465	0.3401	0.3510	0.3586
Log normal	μ	-1.0948	-1.1072	-1.1162	-1.1211
	σ	0.0654	0.0605	0.1444	0.1987

Table 4: Akaike Information Criterion (AIC) and Bayesian Information Criterion (BIC) for C_{fx}

Skin friction coefficient C_{fx}					
Distribution		K =0	K =1	$K = 2$	$K = 3$
Rayleigh	AIC	-245.763	-253.38	-251.87	-248.00
	BIC	-242.694	-250.30	-248.77	-244.87
Frechet	AIC	**-820.387**	-774.23	-521.01	-431.55
	BIC	**-811.181**	-764.98	-511.69	-422.16
Gumbel	AIC	-793.898	-778.29	-523.02	-433.63
	BIC	-787.760	-772.12	-516.81	-427.37
Log-logistic	AIC	-753.396	-781.76	-516.31	-422.59
	BIC	-747.258	-775.60	-510.10	-416.33
Weibull	AIC	-711.008	**-816.70**	**-549.21**	**-454.14**
	BIC	-704.870	**-810.54**	**-543.00**	**-447.88**
Log normal	AIC	-760.185	-798.60	-534.64	-441.59
	BIC	-760.185	-792.43	-528.43	-435.33

Table 5: Parameter estimates for the statistical distribution of Nu_x

Nusselt number Nu_x					
Distribution	Parameter	K =0	K =1	$K = 2$	$K = 3$
Rayleigh	σ	0.3456	0.3530	0.3539	0.3531
Frechet	m	0.0448	0.0428	-5.4444	-5.4444
	s	0.0487	0.0435	5.9444	5.9444
	α	0.5999	0.5558	6.3889	6.3889
Gumbel	μ	0.2137	0.2148	0.2083	0.2029
	β	0.2376	0.2440	0.2451	0.2443
Log-logistic	β	1.4581	1.4088	1.3691	1.3490
	α	0.2146	0.2131	0.2022	0.1941
Weibull	k	1.0472	1.0182	0.9815	0.9595
	λ	0.3709	0.3719	0.3615	0.3530
Log normal	μ	-1.5347	-1.5495	-1.5957	-1.6300
	σ	1.09119	1.1306	1.1630	1.1801

Table 6: Akaike Information Criterion (AIC) and Bayesian Information Criterion (BIC) for C_{fx}

Nusselt number Nu_x					
Distribution		$K = 0$	$K = 1$	$K = 2$	$K = 3$
Rayleigh	AIC	132.3096	152.3221	172.9782	187.1494
	BIC	135.3785	155.4035	176.0842	190.2793
Frechet	AIC	**-25.8300**	**-19.9633**	333.1634	341.5887
	BIC	**-16.6230**	**-10.7191**	342.4812	350.9784
Gumbel	AIC	66.0602	75.4469	80.4107	82.6341
	BIC	72.1980	81.6098	86.6226	88.8939
Log-logistic	AIC	14.7996	21.3907	15.9855	9.6307
	BIC	20.9374	27.5535	22.1974	15.8905
Weibull	AIC	0.0728	4.9620	0.9057	-4.0227
	BIC	6.2107	11.1248	7.1176	2.2371
Log normal	AIC	-5.0487	1.4740	**-4.4967**	**-11.3515**
	BIC	1.0891	7.6367	**1.7151**	**-5.0917**

4.0 Concluding Remarks

The present study evaluates statistical model for the flow and melting heat transfer in microplar nanoliquid over an electromagnetic actuator with variable thickness. The developed model features the effects of viscous dissipation, thermal radiation, temperature-based thermal conductivity. Main equations describing the physical problem are remodeled into ordinary differential equations using appropriate similarity transformation. The resultant equations have been tackled numerically via shooting technique alongside Runge-Kutta Fehlberg algorithm. Various statistical distributions such as Rayleigh, Frechet, Gumbel, Log-logistic, Weibull, Log normal are applied to test the data set of the skin friction coefficient and the Nusselt number for variations in the micropolar nanofluid material parameter. In addition, Akaike Information Criterion (AIC) and Bayesian Information Criterion (BIC) were used to select the best statistical model. The results show that:

- The momentum boundary layer expands with melting heat transfer, modified Hartmann number and fluid material term whereas the fluid velocity decelerates with a rise in the magnitude of the wall thickness parameter.

- The thermal field as well as the temperature boundary layer improves with an increase in the Eckert number, thermophoresis and Brownian motion and micropolar fluid term.
- The data set for the skin friction coefficient fits the Frechet model in the absence of micropolar fluid ($K = 0$) and the Weibull model for $K = 1,2,3$ whereas that of the Nusselt number fits the Frechet distribution for $K = 0,1$ while Lognormal distribution fits for $K = 2$ and 3.
- The statistical model reveals that the form of the distribution for the data sets of skin friction coefficient and Nusselt number change after some values of material micropolar parameter.

References

Aluh, D. O., Onu, J. U. (2020). The need for psychosocial support amid COVID-19 crises in Nigeria. *Psychological Trauma: Theory, Research, Practice, and Policy*. 2020 doi: 10.1037/tra0000704.

Abbas, T., Hayat, T., Ayub, M. Bhatti, M. M, Alsaedi, A. (2017). Electromagnetohydrodynamic nanofluid flow past a porous Riga plate containing gyrotactic microorganism, *Neural Comput & Applic* DOI 10.1007/s00521-017-3165-7

Atif, S. M., Hussain, S. and Sagheer, M. (2019). Magnetohydrodynamic stratified bioconvective flow of micropolar nanofluid due to gyrotactic microorganisms, *AIP Advances* 9, 1-17.

Chen, J., Liang, C. and Lee J. D. (2011). Theory and simulation of micropolar fluid dynamics, J.*Nanoengineering and Nanosystems*, 224, 31-39.https://doi.org/10.1063/1.5085742

Choi SUS. (1995). Enhancing thermal conductivity of fluids with nanoparticles. In: *ASME*, FED 231/MD, 66, 99–105.

Eringen, A. C. (1966). Theory of micropolar fluids. *J. Math. Anal. Appl*., {16}, 1-18.

Eringen, A. C. (1972). Theory of thermo-microfluids, *Journal of Mathematical Analysis and Applications*, 38, 480-496.

Fatunmbi, E. O. and Adeniyan, A. (2018). MHD stagnation point-flow of micropolar fluid past a permeable stretching plate in porous media with thermal radiation, chemical reaction and viscous dissipation. *Journal of Advances in Mathematics and Comp Science*, 26, 1-19.

Fatunmbi, E. O. and Adeosun, A. T. (2020). Nonlinear radiative Eyring-Powell nanofluid flow along a vertical Riga plate with exponential varying viscosity and chemical reaction, *International Communications in Heat and Mass Transfer* 119, 1-10.

Fatunmbi, E. O. and Okoya, S. S. (2020). Heat transfer in boundary layer magneto-micropolar fluids with temperature-dependent material properties over a stretching sheet, *Advances in Materials Science and Engineering*, 2020, 1-11.

Fatunmbi, E. O., Mabood, F., Elmonser, T. and Tlili, T. (2021). Magnetohydrodynamic nonlinear mixed convection flow of reactive tangent hyperbolic nano fluid passing a nonlinear stretchable surface, *Phys. Scr*. 96, 1-13.

Fatunmbi, E. O. and Salawu, S. O. (2021). Analysis of hydromagnetic micropolar nanofluid flow past a nonlinear stretchable sheet and entropy generation with Navier slips, *International Journal of Modelling and Simulation*, 42(3), 359-369.DOI:10.1080/02286203.2021.1905490

Fatunmbi, E. O., Adeosun, A. T. and Salawu, S. O. (2021). Entropy analysis of nonlinear radiative Casson nanofluid transport over an electromagnetic actuator with temperature-dependent properties, *Partial Differentiation Equations in Applied Mathematics*, 4, 1-10.

Gailitis, A. and Lielausis, O. (1961) On possibility to reduce the hydrodynamics resistance of a plate in an electrolyte,

Appl. Magnetohydrodyn. Rep. Phys. Inst. Riga. 12: 143-146.

Gangadhar, K, Kannan, T, Jayalakshmi, P. (2017). Magnetohydrodynamic micropolar nanofluid past a permeable stretching/shrinking sheet with Newtonian heating, *J Braz. Soc. Mech. Sci. Eng.*, .23, 1-13.

Hayat, T., Javed, T. and Abbas, Z. (2009). MHD flow of a micropolar fluid near a stagnation point towards a non-linear stretching surface, *Nonlinear Analysis: Real World applications*, 10, 1514.

Hayat, T., Qayyum, S., Alsaedi , A., Ahmad, B (2018). Mechanisms of double stratification and magnetic field in flow of third grade fluid over a slendering stretching surface with variable thermal conductivity, *Results in Physics* 8; 819–828

Iqbal, Z., Azhar, E., Mehmood, Z. and Maraj, E. N. (2017). Melting heat transport of nanofluidic problem over a Riga plate with erratic thickness: Use of Keller Box scheme, *Results in Physics*, 7, 3648–3658.

Lukaszewicz, G. (1999). *Micropolar fluids: Theory and Applications* (1st Ed.). Birkhauser, Boston.

Mahanthesh, B., Gireesha, B. J., Gorla, R. S. R. and Makinde, O. D. (2018). Magnetohydrodynamic three-dimensional flow of nanofluids with slip and thermal radiation over a nonlinear stretching sheet: a numerical study, *Neural Computing and Applications*, *30*(5), 1557-1567.

Noor, N. F. M., Haq, R. U., Nadeem, S. and Hashim, I. (2015). Mixed convection stagnation flow of a micropolar nanofluid along a vertically stretching surface with slip effects, *Meccanica*, 50, 2007–2022.

Rahman, M. M., Eltayeb and M. R. (2009). Thermo-micropolar fluid flow along a vertical permeable plate with uniform surface heat flux in the presence of heat generation, *Thermal Science*, 13(1), 23-36.

Reena and Rana, U. S. (2009). Effect of Dust Particles on rotating micropolar fluid heated from below saturating a porous medium. *Applications and Applied Mathematics: An International Journal*, 4, 189-217.

Shafq, A., Lone, , S.A., Sindhu, T. N., Al-Mdallal, , Q. M. and Rasool, G. (2021). Statistical modeling for bioconvective tangent hyperbolic nanofuid towards stretching surface with zero mass fux condition, *Scientifc Reports*, 11(1):1-18. Doi:10.1038/s41598-021-93329-y.

Subhani, M and Nadeem, S. (2018). Numerical analysis of micropolar hybrid nanofluid, *Applied Nanoscience*, 9, 447–459. Doi.org/10.1007/s13204-018-0926-2

Xu, L. and Lee, E.W.M. (2013). Variational iteration method for the magnetohydrodynamic flow over a nonlinear stretching sheet. *Abst Appl Anal*, 2013, 1-5.